MATERIALS SCIENCE

"Skin-like" fabric for personal moisture management

L. Lao[1]*, D. Shou[2]*, Y. S. Wu[1], J. T. Fan[1,2†]

Personal moisture management fabrics that facilitate sweat transport away from the skin are highly desirable for wearer's comfort and performance. Here, we demonstrate a "skin-like" directional liquid transport fabric, which enables continuous one-way liquid flow through spatially distributed channels acting like "sweating glands" yet repels external liquid contaminants. The water transmission rate can be 15 times greater than that of best commercial breathable fabrics. This exceptional property is achieved by creating gradient wettability channels across a predominantly superhydrophobic substrate. The flow directionality is explained by the Gibbs pinning criterion. The permeability, mechanical property, and abrasion resistance (up to 10,000 cycles) of the fabric were not affected by the treatment. In addition to functional clothing, this concept can be extended for developing materials for oil-water separation, wound dressing, geotechnical engineering, flexible microfluidics, and fuel cell membranes.

INTRODUCTION

Personal moisture management is essential to thermal comfort and performance. Moisture management fabrics that promote wicking of sweat away from skin are commercially available (*1*, *2*), but such fabrics are not repellent to external liquid water. On the other hand, commercially available breathable fabrics, although water repellent, can only allow a moisture vapor transmission rate up to ~460 g/m^2 per hour (*3*, *4*), which is far less than the sweating rate of an average person under moderate exercise (~1000 g/m^2 per hour) (*5*).

Directional liquid flow phenomena are widely found in nature on insects and plants including beetle's back (*6*, *7*), spider silk (*8*), and cactus branch (*9*), where one-way water collection is driven by the heterogeneous geometry and gradient wettability. Recently, porous materials (e.g., fabrics) allowing transient directional liquid transport have been reported. Such materials were achieved by differential treatment of wettability or lyophilicity across the fabric thickness or combining multilayers of materials with different wettability or lyophilicity as an asymmetric construct (*10*, *11*). In both cases, liquid tends to transport from lyophobic (e.g., hydrophobic or oleophobic) side to the lyophilic (e.g., hydrophilic or oleophilic) side of the material before the lyophilic side is saturated but is blocked in the reverse direction. Different from tuning wettability, our group has recently developed a fluid diode fabric solely made from hydrophilic materials (*12*). The chemistry-free fabric allows one-way liquid transport by optimizing the pore sizes of the multilayer fabric assembly, creating asymmetric breakthrough pressure in different flow directions.

Although the above-reported directional liquid transport (or fluid diode) fabrics can promote the transport of liquid (e.g., sweat) from one side (e.g., the inner next-to-skin side) to the other side (e.g., external surface) for evaporation, the liquid transport rate slows down and the fabrics become heavy and clingy once the outer layer/surface is saturated. In addition, they cannot repel the external liquid contaminants. Here, we present a conceptually novel design strategy by mimicking the master of sweat regulation—human skin. Human skin is an ideal directional liquid flow material as it excretes liquid sweat and protects the body from external liquid contaminants (Fig. 1A) (*13*, *14*). In this study, we developed a "skin-like" directional liquid transport fabric, which allows continuous one-way water flow and repels external liquid. This is achieved by endowing gradient wettability in spatially distributed porous channels on a predominantly hydrophobic fabric. We used a hydrophilic cotton fabric as a starting material and pretreated it with 1*H*,1*H*,2*H*,2*H*-perfluorooctyltriethoxysilane (PFOTES)–coated titanium dioxide (TiO_2) nanoparticles to impart superhydrophobic finishing (*15*). Selective plasma treatment via a patterned mask was then applied to create porous gradient wettability channels across this hydrophobic fabric (Fig. 1B), acting as localized sweat glands. While these channels serve for one-way liquid flow, the predominantly superhydrophobic nature of the fabric makes it expel the transported liquid or external liquid from the surface. This skin-like fabric has great potentials to various applications such as functional clothing (*16*, *17*), oil-water separation (*18*, *19*), wound dressing (*20*, *21*), geotechnical engineering (*22*, *23*), flexible microfluidics (*24*, *25*), and fuel cell membranes (*26*).

RESULTS

Wettability, microstructure, and chemical properties of the fabric

We first checked the wetting behavior of the fabric before and after superhydrophobic finishing and successive selective plasma treatment. As shown in Fig. 2A, the superhydrophobic finished fabric showed a contact angle (CA) of 152°, while that of the pristine cotton fabric is 0° (superhydrophilic; fig. S1). The increased hydrophobicity was endowed by the surface nanostructures of the perfluorosilane-coated TiO_2 nanoparticles (*15*). When the fabric was treated by the plasma etcher, a notable difference in the CA between exposed spot and unexposed nonspot areas was created. The CAs of the unexposed areas on both top and back sides of the fabrics only decreased slightly and still stayed at high values. This is due to the coverage of the tape mask, which prevents the O_2 plasma going inside the fabric to endow hydrophilicity (*27*). On the contrary, the CAs of the exposed spot areas on both top and back sides of the fabric decreased markedly with the increase of plasma treatment time. For instance, 1-min treatment brought the CA of the spot areas on the top side of the fabric down to 135°, which further decreased to 114° after 2 min, 97° after 3 min, and 44° after 5 min. The CA change of the spot areas on the back side of the fabrics was interesting, which dropped down to 141° after 1 min, but was no longer measurable (N/A, noted as 0°)

[1]Department of Fiber Science & Apparel Design, Cornell University, Ithaca, NY 14853, USA. [2]Institute of Textiles and Clothing, Hong Kong Polytechnic University, Hunghom, Kowloon, Hong Kong.
*These authors contributed equally to this work.
†Corresponding author. Email: jf456@cornell.edu; jin-tu.fan@polyu.edu.hk

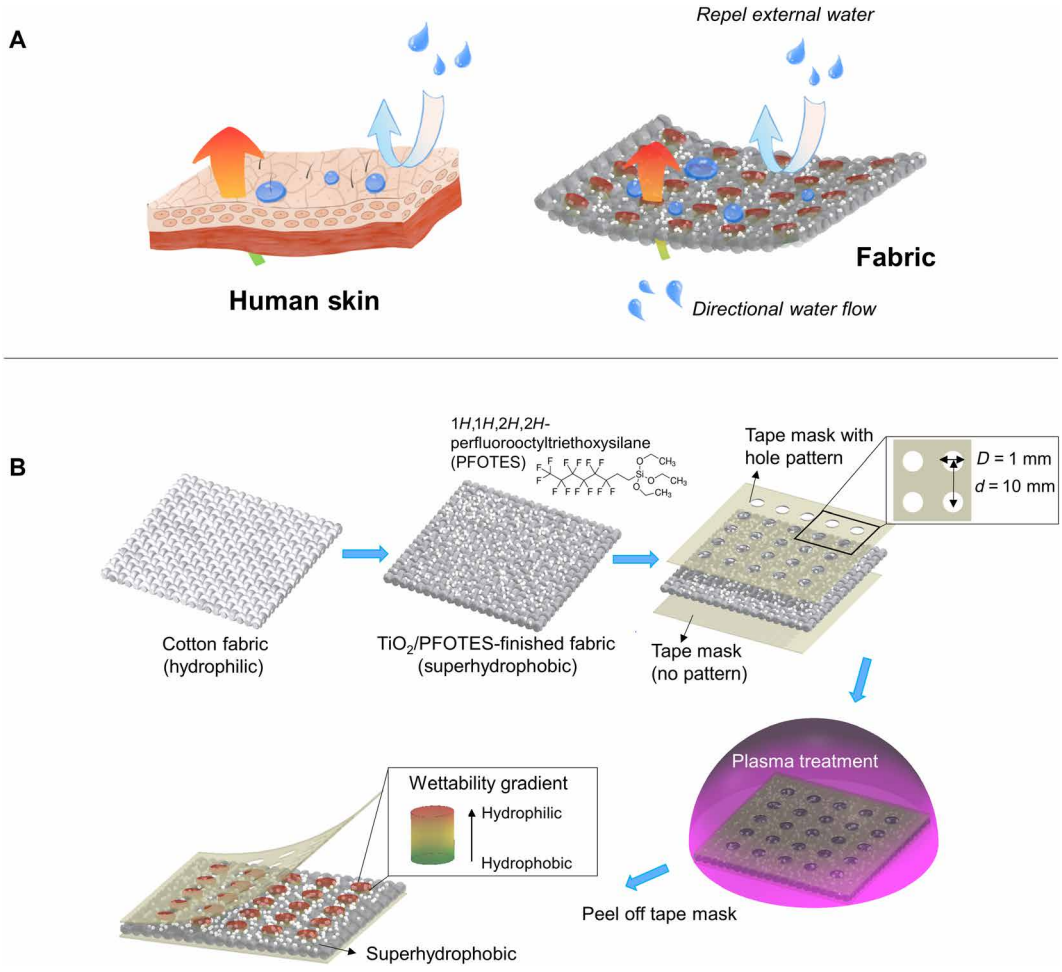

Fig. 1. Schematic illustration and fabrication process of a skin-like fabric with both directional water transport and water repellency. (**A**) Schematic demonstration of the dual properties of the skin-like fabric. (**B**) Combination of superhydrophobic finishing via perfluorosilane-coated TiO_2 nanoparticles and selective plasma treatment via a patterned mask to create gradient wettability spot channels through the fabric thickness to endow the dual properties.

after 2 min or longer. This is because the water droplets transported quickly from the back spot areas to the top spot areas (Fig. 2A, inset images, and fig. S1); therefore, a zero CA value was recorded. A series of dynamic CA images can be found in fig. S2 when 10-μl water droplet was placed on either side of the plasma (300 W, 3 min)–treated superhydrophobic fabric. When water was dripped onto the plasma-exposed top spot area, the droplet stayed on the surface steadily for 3 s and longer time, with an average CA of 97° (fig. S2A). However, when it was dripped on the reverse side (unexposed back spot area), the droplet quickly transported to the other side (top side) of the fabric (fig. S2B); for other nonspot areas on both sides, the round water droplets were still kept there (fig. S2, C and D). A dynamic process of directional water transport can be further viewed in movie S1 (A and B), where a 20-μl water droplet was manually dripped from the pipette onto top and back spot areas of the fabric, respectively.

To measure the "real" CAs of the spot areas on the back side of the fabric after plasma treatment, we assembled two layers of the superhydrophobic finished fabric and then covered the top and back sides of the assembly with the patterned tape mask (Fig. 2B, inset image) and treated it with plasma. We then measured the CAs of the spot area on the top side of the second layer and used it as the "real" CAs of the spot area on the back side of the first layer, with the assumption that they should be similar as the two layers are closely stuck (*28*, *29*). Figure 2B shows that CAs decreased gradually along with the plasma prolongation, but they are far above "zero," e.g., 109° for the sample after 3-min plasma treatment. This means that plasma penetrated into the spot channels and decreased the hydrophobicity to different degrees, forming a wettability gradient through the fabric thickness. Notice, for the samples with less than 3-min treatment, both top and back spots were still hydrophobic (CA over 90°), whereas the sample with 5-min treatment became hydrophilic on both sides through the spot (also see fig. S1). This may explain the hanging round droplet appearances for the transported water droplets on the opposite (top) side for the 2- and 3-min samples and a spreading shape for the 5-min sample (Fig. 2A, inset images, and fig. S1). The CAs of the plasma-treated fabrics were also measured after 7 days' aging at room temperature (fig. S3A), and they showed the similar trends as those at day 0 (Fig. 2A), indicating that the samples were stable. In addition, the water transport time from the back spots to the top spots decreased with the prolongation of plasma treatment, e.g., ~ 5 s for the as-prepared 2-min plasma-treated fabric,

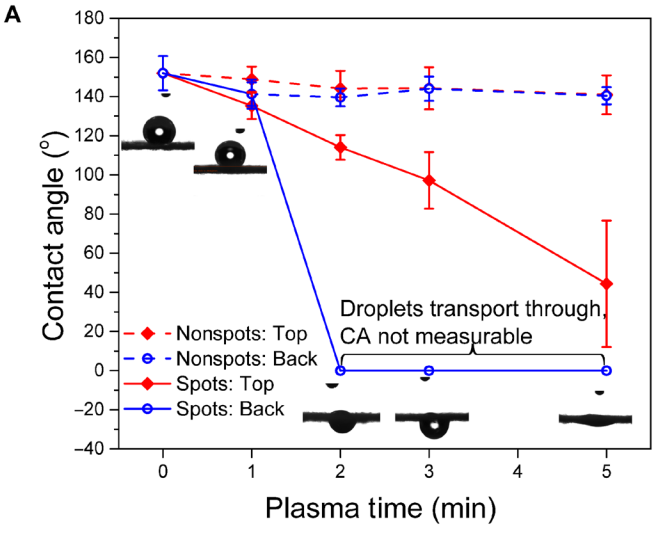

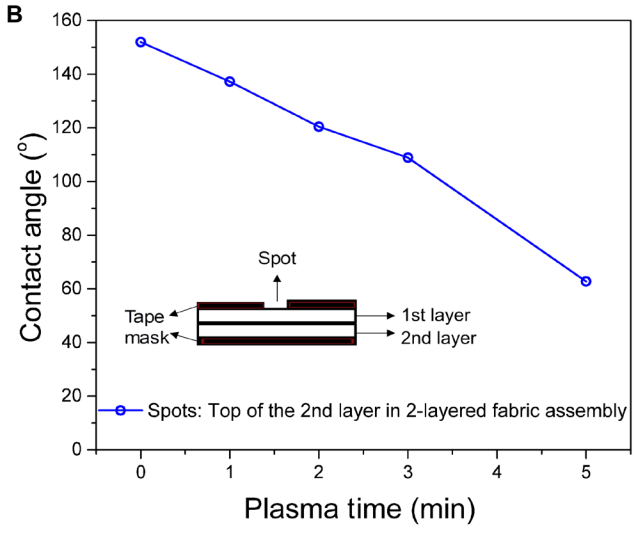

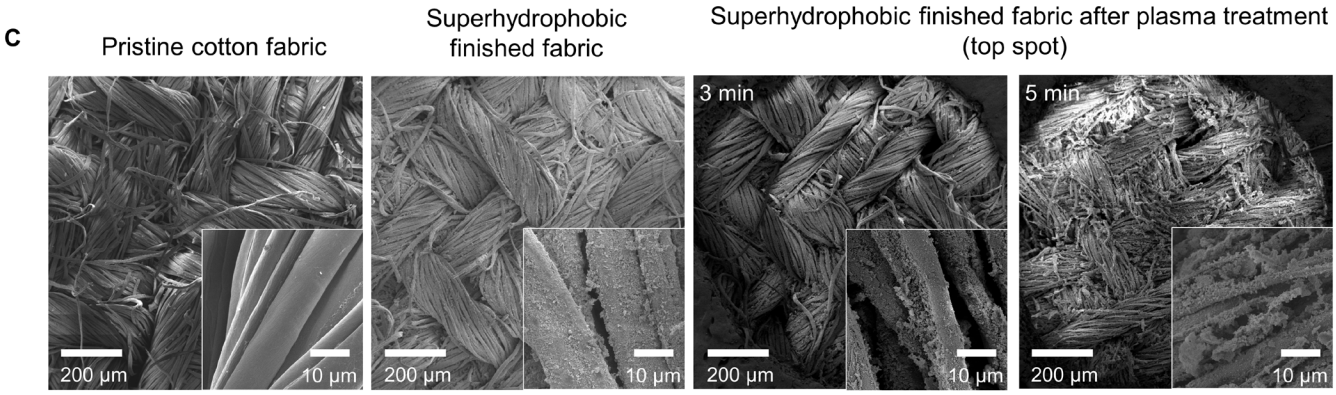

D

Sample	C (%)	O (%)	Ti (%)	Si (%)	F (%)
Pristine cotton fabric	62.89	35.17	0.16	1.11	0.67
Superhydrophobic finished fabric (top)*	28.18	28.42	7.88	0.99	34.53
Superhydrophobic finished fabric (back)*	27.37	32.38	6.27	0.44	33.54
After plasma 3 min (top spot)	42.77	47.51	7.37	1.43	0.91
After plasma 3 min (back spot)	40.39	35.89	6.41	1.95	15.36

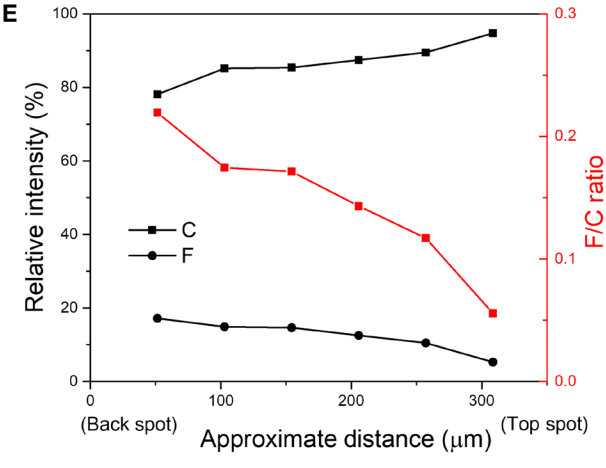

Fig. 2. Wetting behavior, microstructure, and chemical analysis of the superhydrophobic finished fabric after selective plasma treatment. (**A**) CAs of the spot and nonspot areas of both top and back sides of the superhydrophobic finished fabric after plasma treatment for 0 to 5 min; insets are droplet images when dripped on the back spot areas. (**B**) CA of a two-layer fabric assembly to prove the wettability gradient. (**C**) SEM morphologies of pristine cotton fabric, superhydrophobic finished fabric, and exposed top spot areas of the superhydrophobic finished fabric after selective plasma treatment for 3 and 5 min. (**D**) Table of atomic contents of C, O, Ti, Si, and F on different fabric surfaces from XPS survey results. *One side of the superhydrophobic finished fabric is marked as top side, and the other is marked as back side. (**E**) C and F relative intensities and F/C ratios across the thickness of treated fabric (from the back spot area to the top spot area) from iXPS test.

about 1 s for the 3-min sample, and below 1 s for the 5-min sample, and the samples after 7 days' aging only slightly increased the transport time at each corresponding condition (fig. S3B). Overview images of multiple water droplets on either side of the treated fabric at days 0 and 7 can be found in fig. S3C.

Figure 2C shows the typical scanning electron microscopy (SEM) morphologies of the fabric after different treatments. Compared with a smooth fiber structure on the pristine cotton fabric, the superhydrophobic finished fabric showed a rougher fiber surface because of the TiO_2 nanoparticles. The top spot area of the fabric treated by plasma for less than 3 min still kept clear yarn structure, but those treated for more than 5 min generated fuzzy surfaces and broken fibers. The back spot areas have a similar morphology trend as the top area (fig. S4), indicating that plasma, besides the surface treatment on the top spot areas, can penetrate through the thickness via spot channels. All the unexposed nonspot areas on both top and back sides did not change the fibrous morphologies (fig. S5) because of the coverage by the tape mask. Combining the water transport screening by the CA test (Fig. 2A) and SEM morphologies (Fig. 2C), we chose the superhydrophobic fabric after selective plasma treatment under 300 W for 3 min for further studies.

X-ray photoelectron spectroscopy (XPS) was then used to investigate the chemical elements of the fabrics before and after superhydrophobic finishing and plasma treatment (300 W, 3 min). As shown in the table of Fig. 2D, both the titanium (Ti) and fluorine (F) content increased after the TiO_2/PFOTES superhydrophobic finishing on the cotton fabric. The superhydrophobic finishing was uniform, as both sides showed identical component content, with an average F of 34.04%. After selective plasma treatment, the Ti content kept stable on both top and back spots, which coincides with the thermogravimetric analysis (TGA) data (fig. S6) and identical rough morphology on the corresponding areas (Fig. 2C and figs. S4 and S5). However, there was a significant difference in F content, which decreased to 0.91 and 15.36% on the exposed top and unexposed back spot areas, respectively. This indicates that the fluorine-based hydrophobic silane chains on the exposed top spot areas might be severely etched away by the plasma (*30*), and those underneath the spots were also damaged by the penetration of the plasma through the thickness via spot channels but in a less severe extent. Similar observation was also reported by Wang *et al.* (*29*, *31*). The cross-sectional image XPS (iXPS) further confirmed this speculation, as the relative intensities of F and C decreased and increased, respectively, in the back spot to top spot direction, which results in a decreasing F/C ratio from 0.22 near the back edge to 0.06 near the top edge (Fig. 2E). The indication of plasma penetration and diminishing the fluorine chains coincides with the SEM trend (Fig. 2C) and CA trend for either the one-layer (Fig. 2A) or two-layer structures (Fig. 2B), which confirms the gradient wettability and explains the directional water transport within the spot channel area.

Directional water transport and water-repellent properties of the fabric

To confirm the dual directional flow property and water repellency, the fabrics were placed at an inclined angle of 45°, and water was dripped from either top or back spot areas of the fabric by a needle connecting with a continuous water source at a flow rate of 10 μl/min. Figure 3A shows a series of photos captured during these experiments (movie S2, A and B). When water was dripped from the top side of the fabric, it first adhered to the spot area, e.g., first droplet at 5.0 s. During the continuous supply with water, the droplet grew, and after the last droplet at 280.8 s, it was big enough (~46 μl) to roll off from the fabric. Through the entire process, no water penetration was observed. In the reverse direction, when the first droplet contacted the back spot area, it spontaneously transported from the pin of the needle to the other side after 10.0 s, and after accumulating to a similar volume at 248.5 s, the large droplets roll off again from the top surface. From this test, we can estimate the maximum flow rate of each channel to be 46/248.5 = 0.185 μl/s. In one of our test specimens, the spatial distance of the channels is 1 cm, so the maximum water transport rate is $0.185 \times 0.001\ g \times 3600/0.0001\ m^2$/hour = 6660 g/$m^2$ per hour, which far exceeds the maximum sweating rate of an average person under strenuous activity and is about 15 times greater than that of the best commercial Gore-Tex fabric (*3*).

The breakthrough pressures of the top and back sides of the designed fabric with one spot were also experimentally examined via a water flux test by placing a plastic hollow cylinder on either side to hold water (fig. S7A) (*12*). We first examined the fabrics with different spot sizes at a flow rate of 0.4 ml/min, as shown in Fig. 3B. Apparently, there is a difference of the breakthrough pressures for the top and back sides of the fabric. For the top sides, the pressures were higher and decreased with the increase of the spot sizes, i.e., the smallest spot size (diameter) of 0.5 mm generated a 4.7cm H_2O pressure, the medium size of 1 mm reduced the pressure to 3.76 cm H_2O (also see movie S3A), and the biggest size of 3 mm further reduced to 1.8 cm H_2O. This is reasonable, as a bigger plasma-exposed area would enlarge the channels for the water to pass through, thereby lowering breakthrough pressure. When the fabrics were placed inversely (back side up), the supplied water droplets can quickly transport through, resulting in a very low breakthrough pressure, ~0.2 cm H_2O (see movie S3B for the sample of spot size 1 mm). Besides, we tested the fabric with a spot size of 1 mm at different flow rates and found that the pressure increased with the increase of the water flow rates (Fig. 3C), which should be caused by the delay of liquid penetration considering the predominantly flow resistance of the fabrics (*12*). In addition, we also recorded the droplet sizes of the water transported through the spots and found that they increased with the spot enlargement (fig. S7B).

The directional water transport ability was further proved by showering either the top or back side of the fabric capping over a glass vessel loaded with blue silica gel beads (fig. S8A). After the vessel was showered using an eye wash shower for 10 s, the color of the inside beads did not change when the top side of the fabric was capped upside (fig. S8B), whereas it partially turned to pink when the back side was capped upside (fig. S8C), indicating a water transport through the fabric into the vessel.

Besides water, we also used artificial sweat [prepared according to International Organization for Standardization (ISO) 3160-2, containing NaCl (20 g/liter), NH_4OH (17.5 g/liter), acetic acid (5 g/liter), and lactic acid (15 g/liter), with the pH adjusted to 4.7 by NaOH] to test the directional transport properties of the fabrics at a flow rate of 10 μl/min. The fabrics were originally laid horizontally. As shown in Fig. 4A, when sweat droplet was dripped on the top spot of the fabric, it stands firmly on the surface and did not transport through. We then rotated the fabric clockwise to inclined angles while continuing to supply sweat droplets and found that the growing droplets rolled off at an angle of 47° (movie S4A). For the back spot of the fabric, we fed the sweat droplet upward to test the transport behavior against the gravity. As shown in Fig. 4 (B and C), when the first droplet

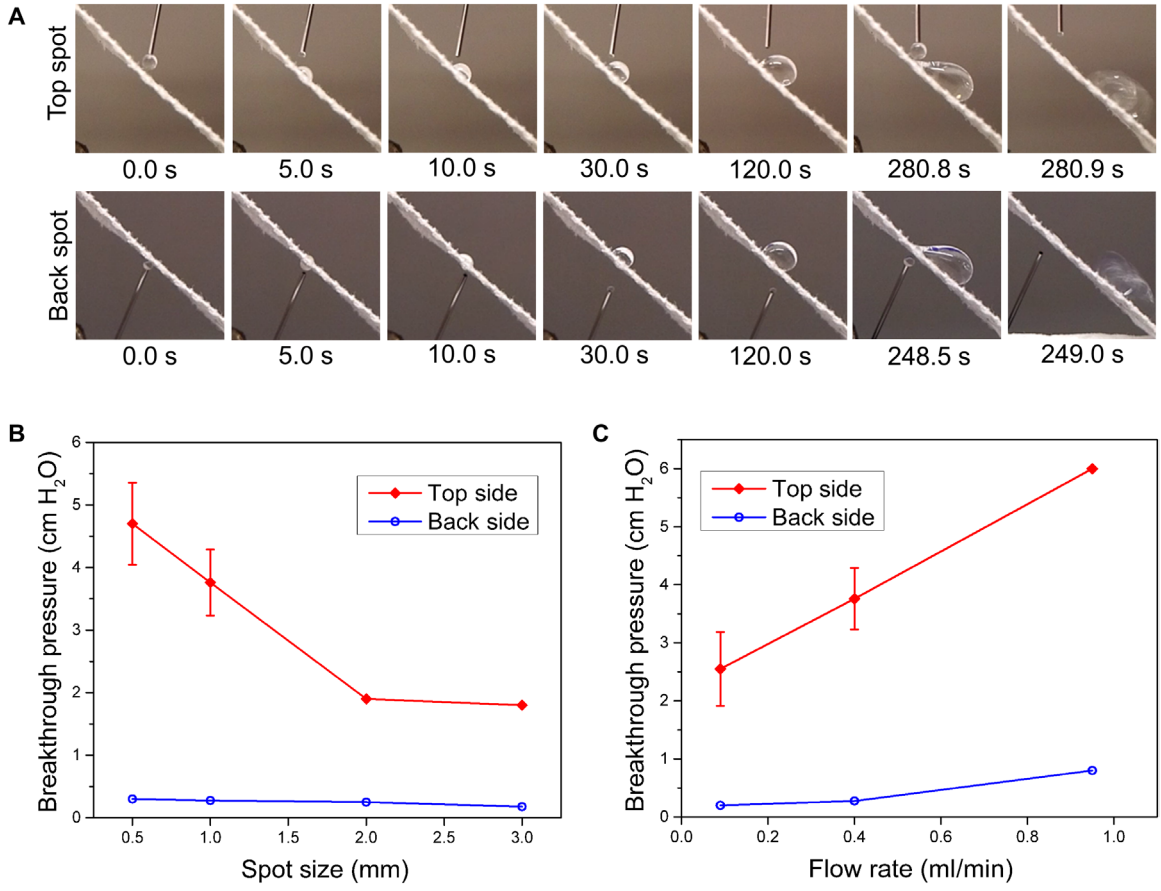

Fig. 3. Directional water transport property and water repellency of the superhydrophobic finished fabric after selective plasma treatment. (**A**) Still frames taken from videos when water was dripped onto an inclinedly laid (45°) plasma selectively treated superhydrophobic finished fabric on exposed top spot and unexposed back spot areas under a flow rate of 10 μl/min. (**B** and **C**) Breakthrough pressures of both top and back sides of the fabrics versus (B) different sizes (diameters) of spot areas under a flow rate of 0.4 ml/min and (C) different flow rates through a spot diameter of 1 mm. Movie credit: Lihong Lao, Cornell University.

contacted the back spot area, it can also spontaneously transport to the top surface to half of the volume (movie S4, B and C), indicating that the transport ability comes from the capillarity force, but the force is insufficient to overcome the gravity. Successive supplies showed the similar behaviors, with half of the volume transported to the top surface and another half hanged on the back spot area. Rotating the fabric to increase the inclination angle helps the complete transport of the growing droplet to the top surface, which eventually dropped off at an angle of 63° (movie S4B). The inclined angles for the final roll-off of the sweat droplet was larger compared to that for the water droplet (45°), probably because artificial sweat liquid has a higher surface tension due to the large amount of the ions (*32*, *33*).

Breathability, mechanical property, and abrasion resistance of the fabric

In addition, we tested other properties of the cotton fabric before and after superhydrophobic finishing and selective plasma treatment, e.g., breathability, mechanical property, and durability. We found that the superhydrophobic finishing and plasma treatment did not have a detrimental effect on the water vapor transmission rate (WVTR) under 35°C (fig. S9A) and air permeability (fig. S9B), but they increased the tensile strength and modulus due to the nanoparticle incorporation (fig. S10), which is consistent with our previous study (*34*). When the fabric was abraded under different cycles, the CA of the predominant nonspot areas slightly decreased after shorter cycles, e.g., ~139° after 10,000 cycles ($P > 0.05$), and further decreased to ~116° with prolonged 25,000 cycles ($P < 0.05$) (fig. S11A). Regardless, the TiO_2 nanoparticles remained a similar content (~8%) as that of the fabric before abrasion (fig. S11A), indicating the robustness of the nanoparticle coating on the fabrics (*15*). SEM showed that there were increased breakages of the fibers for both pristine cotton fabric and plasma-treated superhydrophobic fabric along with the abrasion cycles (fig. S11B), which should be the reason of reduced wettability, as more hydrophilic cotton fiber cross sections are exposed on the surface. Overall, the treated fabric showed a good abrasion resistance up to 10,000 cycles. In addition, we also tested the durability of the transport properties of the treated fabric after 5 weeks' aging at room temperature and found that water was still able to transport from the back spot area to the top spot area and repel in the reverse direction (fig. S12).

MECHANISM UNDERSTANDING AND DISCUSSION

A theoretical basis has been proposed to explain the design approach and understand the mechanisms of the directional water transport and the release of water drops from the fabric surface. The dependence

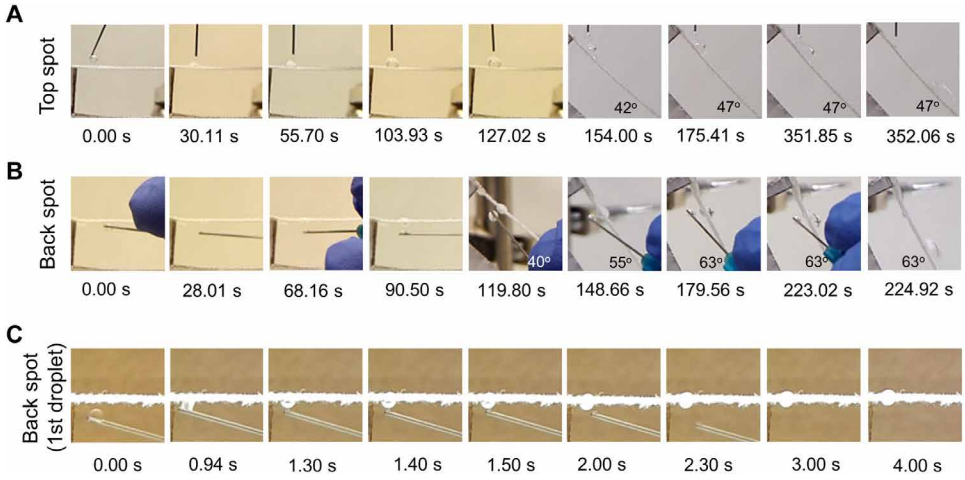

Fig. 4. Directional transport property and repellency of artificial sweat liquid on the superhydrophobic finished fabric after selective plasma treatment. (**A** and **B**) Still frames taken from videos when sweat droplet was dripped onto (A) exposed top spot and (B) unexposed back spot areas under a flow rate of 10 μl/min. The fabrics were originally laid horizontally and then were rotated clockwise to certain inclined angles. The back spot was tested via dripping sweat liquid initially upward against the gravity. (**C**) Transport behavior of a first sweat droplet when being dripped upward to the back spot of the horizontally laid fabric. Movie credit: Lihong Lao, Cornell University.

of the flow directionality and the breakthrough pressure on the microstructure and wettability of the fibrous systems has also been analyzed.

Water transport by liquid drops is much faster than that by vapor evaporation, while one water drop contains millions of vapor molecules. The underlying principle of the fluid directionality in the porous spot with gradient wettability is illustrated in Fig. 5A. Here, the Gibbs pinning criterion, which has been successfully correlated to the flow directionality in the fibrous fluid diodes with varied geometry (*12*), is extended to describe the directional water transport inside the hollow channels between yarns with both gradient wettability and varied microstructure. Because the channel between the yarns varies in size along the flow direction, an expansion/contraction angle (α) is used to characterize the degree of the expansion or contraction of flow path (Fig. 5B). When the channel is uniform in size, α becomes zero, and α approaches 90° or −90°, respectively, at the bottom and top of the fibrous material in the flow direction. More specifically, the contact line gets pinned with the breakthrough angle α + θ beyond 90° based on the Gibbs pinning condition (*12*). On the contrary, the advancement of the liquid continues when the air-liquid interface is concave and the dragging force exists toward the flow direction. As such, continuous advancement of the liquid water can be satisfied, when the direction angle β as a function of CA θ and the expansion/contraction angle α are satisfied as follows

$$\beta = \alpha + \theta - \frac{\pi}{2} < 0 \quad (1)$$

It can also be seen from Fig. 5B that liquid water will flow inversely if β > 0, as the driving force on the basis of surface tension becomes opposite to the intended flow direction. Assuming that the yarns are elliptical, their surface can be described as the locus of all points that satisfy the equations, viz., $x = a\cos\omega$, and $y = b\sin\omega$, where x and y are the coordinates of any point on the ellipse; a and b are the semi-axes in the x and y directions, respectively; and ω is the angle of eccentric anomaly, which ranges from π/2 to −π/2 radians in Fig. 5B. The value of α can be determined by the slope of the tangent line at ($a\cos\omega$, $b\sin\omega$) to the ellipse, viz., $\alpha = \arctan\left(\frac{1}{k}\right)$, where $k = -\frac{b}{a}\frac{\cos\omega}{\sin\omega}$.

It has been shown in Fig. 2B that the bottom surface (back side) of the porous spot becomes less hydrophobic with increasing time of plasma treatment. Here, a linear gradient of wettability is assumed from the hydrophilic (simplified as "I") top spot surface with CA at 0° when ω = π/2 to the hydrophobic (simplified as "O") bottom surface with CA at θ_0 when ω = − π/2, with $\theta = \theta_{IO} = -\frac{\theta_0}{2}\sin\omega + \frac{\theta_0}{2}$. In the opposite flow direction, the CAs will be $\theta_{OI} = \frac{\theta_0}{2}\sin\omega + \frac{\theta_0}{2}$ with CA at 0° when ω = − π/2 to the bottom surface with CA at θ_0 when ω = π/2. The maximum value of the CA on the face away from plasma exposure is obtained as $\theta_0 = 109^o$ for the sample with 3-min treatment (Fig. 2B). The dependence of the diode effect on ω that indicates water advancement is shown in Fig. 5A, where the sign "block" indicates that the flow ceases or retreats at the local area, while the sign "pass" means that the flow can continue moving. It is found that the values of a and b in Eq. 1 are approximately 80 and 50 μm, respectively, and c is approximately 50 μm (fig. S13). Note that the surface tension force is always aligned with the flow direction at β < 0, when the water flows from the hydrophobic side to the hydrophilic side as seen in Fig. 5C. It can be readily understood that the effect of marked contraction leading to high α (negative) overcomes that of the fair hydrophobicity with $\theta_{OI} > 90^o$ at the beginning stage and in the rest of the flow process, while the condition of β < 0 is always satisfied with the reduction of θ_{OI}. In the adverse flow direction, the condition of β < 0 is also secured at the beginning with α < 0 and $\theta_{IO} \sim 0$. However, β eventually becomes positive and the surface tension force is opposite to the main flow direction, with continuously increasing α (positive) and θ_{IO} during the progress of water movement. As such, the asymmetric flow behaviors from different flow directions result from the changes of the geometrical structures and gradient wettability of the fibrous systems, as revealed by the theoretical model of Eq. 1 and experimental findings in Fig. 3. The dependence of direction angle on eccentric anomaly of the elliptical yarns in different flow directions has been further studied in fig. S14, when the semi-major axis and semi-minor axis vary at different values of the maximum CAs of one surface of the porous spot (i.e., $\theta_0 = 109^o$ and $\theta_0 = 170^o$). Both flows can be hindered from two different directions for $\theta_0 = 170^o$ when b = 80 μm and a = 50 μm, because the CA of the

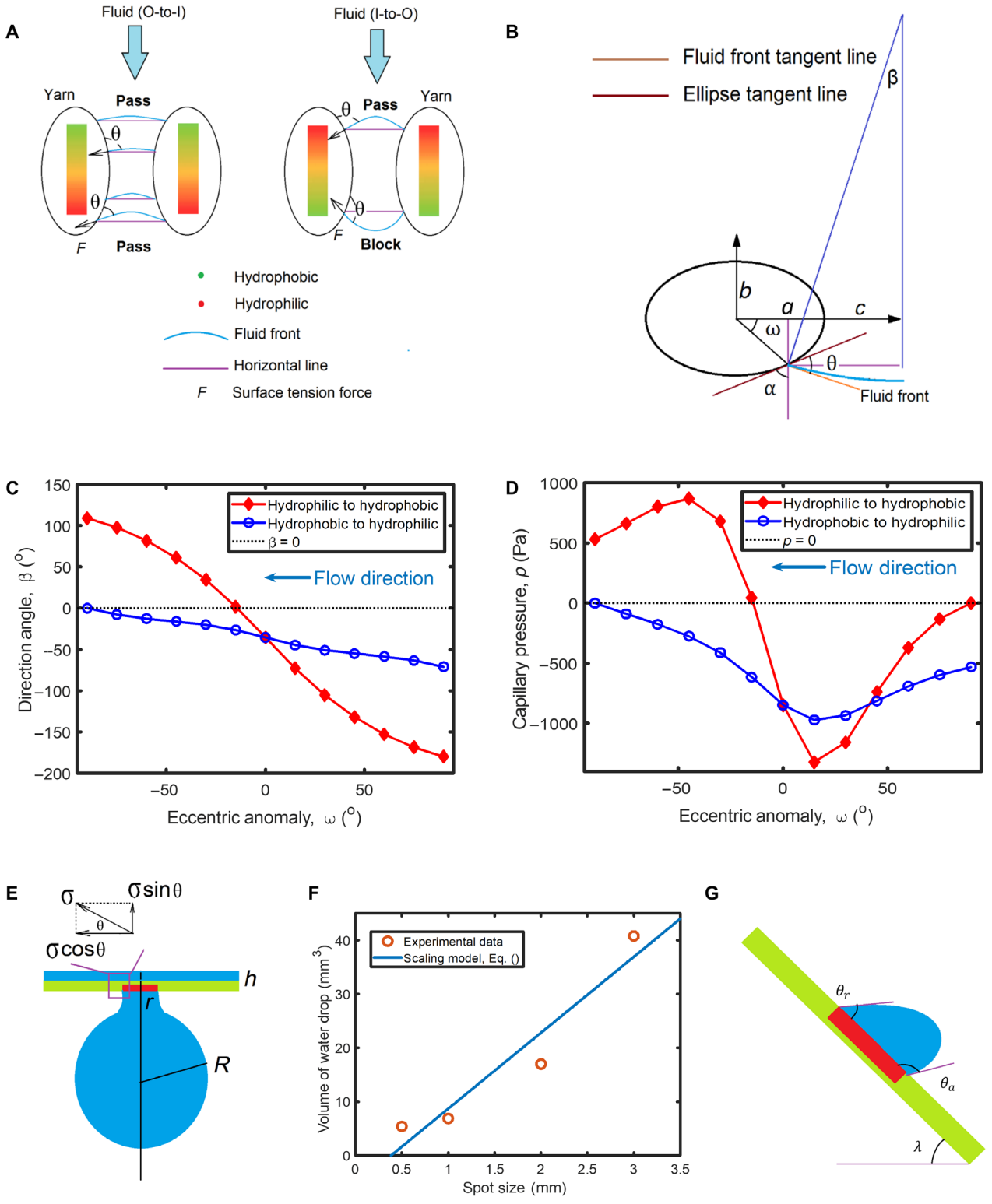

Fig. 5. Mechanism of directional water transport. (**A**) Illustration of directional water transport through the spot channel between elliptical yarns with gradient wettability. (**B**) Illustration of an axisymmetric water fluid front between elliptical yarns. Here, *a* and *b* are the semi-principal axes in *x* and *y* directions, respectively; *c* is the half-distance between yarns; θ is the CA; ω is the eccentric anomaly; α is the expansion/contraction angle; and β is the direction angle. (**C**) Dependence of direction angle on the eccentric anomaly of the elliptical yarns in different flow directions. (**D**) Dependence of capillary pressure on the eccentric anomaly of the elliptical yarns in different flow directions. (**E**) Mechanical analysis of the water drop hung under the porous spot of the horizontally placed fibrous layer with increasing water supply. (**F**) Relationship between the size of the porous spot and the volume of the dripped water drop. (**G**) Mechanical analysis of the water drop attached on the porous spot of the inclined fibrous layer at an inclined angle of λ.

yarn surface is always high in a wide area, where the expansion/contraction angles keep close to zero.

The detachment of water drops is essential to the continual directional water transport process. In this work, patterned hydrophilic porous spots are distributed on the predominately superhydrophobic surface for easy water removal. The size and wettability of the spots are related to the breakthrough pressure and detachment of water drops. It is noted that the capillary pressure varies at different positions of fluid fronts, and the maximum value of capillary pressure that blocks the water transport will be equal to the breakthrough pressure. The capillary pressure within the channel between yarns is determined by the Young-Laplace equation

$$P = \frac{\gamma \sin\left(\alpha + \theta - \frac{\pi}{2}\right)}{L} \quad (2)$$

where $L = a + c - a\cos\omega$ is the half-distance of the width of the fluid front and c is the half-distance between yarns. It is clear that the capillary pressure is all negative in the *OL* flow direction in Fig. 5D (and fig. S15A), so the breakthrough pressure will be equal to zero consistently with the advance of the liquid water. From the opposite flow direction, a positive capillary pressure is found with the maximum value at 800 Pa (8.16-cm water head). This capillary pressure is greater than the 3.76-cm water head shown in Fig. 3B, possibly because some porous spots contain larger channels with greater c (see red arrow in fig. S13B), leading to the reduction in capillary pressure. With increasing a while keeping b and c constants, fig. S13B reveals that a flatter shape of elliptical yarn can yield a lower breakthrough pressure. Besides, more hydrophobic porous spots with higher θ_0 leads to an increase in breakthrough pressures, as seen in fig. S15C.

With increasing water supply, the volume of water drops increases until they fall off from the porous spot, with the gravitational force overcoming the surface tension. The contacting circle interface line among the air, the water drop, and the fabric cannot enlarge due to the repellence of the surrounding hydrophobic regions (Fig. 5E). Thus, the corresponding surface tension drag is equal to $F_a = 2\pi r\sigma\sin\theta$, where r is the radius of the hydrophilic porous spot and $\theta < 90^o$. Then, the drag will be balanced with the critical gravitational force of the growing water drop, which has a weight of $G = \rho g(4\pi R^3/3)$. Thus, we have the scaling law accounting for the relationship between r and R based on $F_a = G$, viz.

$$r \sim R^3 \quad (3)$$

which holds until the detachment of the water drops. Equation 3 has been well verified by the experimental results of detachment of water drops at different sizes of porous spots (Fig. 5F, also see fig. S7B).

When the fibrous layer is placed at an inclined angle at $\lambda = 45^o$, the surface tension drag is generated by the hydrophilic and hydrophobic areas, $F_a = \pi\gamma R_f(\cos\theta_r - \cos\theta_a)$, where θ_a and θ_r are the advancing and receding CA, respectively (Fig. 5G). The hydrophilic force in the upper area of the porous spot holds the water drop, and the hydrophobic force in the lower region repels and impedes the water drop from rolling off. The gravitation force of the water drop is scaling to $mg\sin\lambda$, which will be equal to the capillary forces at the detachment condition, viz.

$$mg\sin\lambda \sim \pi\gamma R_f(\cos\theta_r - \cos\theta_a) \quad (4)$$

where the mass of water drop scales with the cubic drop radius R_f, viz., $m \sim R_f^3$. Analogous to the phenomenon described in Eq. 3, the increase in m is much faster than that of R_f in Eq. 4, which explains the fact that the detachment of growing water eventually drops. The directional water transport will stop if the Laplace pressure of the supplied water drop is equal to the hydrostatic pressure of the water column or water drop generated in the other side of the fabric (*35*). However, this condition cannot be met in reality as the water drop will fall off when growing slightly big.

CONCLUSION

In summary, we have developed a novel skin-like fabric with both directional water transport and water repellency. We created spatially distributed porous spot channels with gradient wettability across the thickness of hydrophobic fabrics via a combination of superhydrophobic finishing and selective plasma treatment. While these channels serve for directional liquid transport, the predominantly untreated surface area remained superhydrophobic, therefore repelling external liquid contaminants. The mechanism of directional flow is explained by the Gibbs pinning criterion. The superhydrophobic finishing and plasma treatment have no detrimental effect on the breathability, mechanical property, and abrasion resistance (up to 10,000 cycles) of the fabric. The technology may be applicable for all kinds of fabrics. Either the hydrophobic prefinishing or selective plasma treatment is simple and efficient; therefore, it will be very feasible for commercial applications. The novel skin-like fabric can have a direct application in developing smart and high-performance clothing, especially for sportswear, bringing a huge value for the industry and consumers. The technology may also be extended to develop fabrics or membranes for other applications where directional liquid transport are needed, such as liquid separation and purification, fuel cells, and flexible microfluidic devices. In addition, the fluorochemicals used for superhydrophobic finishing may be replaced with biosafe chemicals, such as polydimethylsiloxane copolymers, in future development of materials for biomedical applications.

MATERIALS AND METHODS

Superhydrophobic finishing of cotton fabric

The fabrics used for the experiment were woven cotton fabrics. They were treated via conventional desizing, scouring, and bleaching process before their use (*36*).

The superhydrophobic coating was prepared using the following protocol (*15*). Two grams of PFOTES ($C_{14}H_{19}F_{13}O_3Si$, 97%; Oakwood) was dissolved in 198 g of ethanol via vigorous mixing for 2 hours. The solution was subsequently mixed with 10 g of Degussa P25 TiO_2 nanoparticles (rutile/anatase, 85:15; 99.9%; 20 nm; Degussa) to form a suspension. The cotton fabrics with designed sizes were immersed in the coating suspension for 5 min and dried in air for 10 min before testing.

Selective plasma treatment of the finished fabric

One side of the superhydrophobic finished cotton fabric (notated as top side) was tightly covered by a layer of paper tape mask with laser-cut hole patterns (diameter varies from 0.5 to 3 mm, with a typical one of 1 mm, and the intervals between holes are 10 mm); another side (notated as back side) was covered by the same tape mask without the hole patterns (Fig. 1B). The masked fabric was placed

into an oxygen gas plasma etcher (PE100RIE, Plasma Etch Inc.) and treated under an O_2 flow rate of 50 cm^3/min and a power of 300 W for a certain time. Because of the patterned mask, only the hole spot area of the top side of the fabric was expected to be exposed to the plasma. After plasma treatment, the tape mask was peeled off from both sides of the fabric.

Characterization

CA measurement

CAs of the fabrics were measured via the sessile drop method using the Video Contact Angle (VCA) System (AST Products, Billerica, MA) equipped with the software (VCA Optima XE). The fabrics were cut into strips and hung in the air by fixing two ends using a thick (~8 mm) epoxy putty tape on a glass slide. A 10-μl water droplet was placed on the fabric surface to check either its CA or the transport properties. At least five parallel measurements from both spot and nonspot areas on both sides of the fabrics were conducted on each specimen, and the results of either CAs or transport time were averaged for each fabric sample.

Morphology analysis

SEM (Tescan Mira3 FESEM) was used to study the microstructure of the cotton fabric before and after superhydrophobic finishing and selective plasma treatments. The samples were coated with a thin layer of gold palladium before observation.

Chemical analysis

The surface chemical information of the cotton fabrics before and after superhydrophobic finishing and plasma treatment were analyzed by XPS, using an SSX-100 ESCA spectrometer (Surface Science Instruments) with operating pressure of ca. 2×10^{-9} torr. Monochromatic Al Kα x-rays ($h\nu$ =1486.6 eV) were generated at a power of 200 W (10 mA; 20 kV). Photoelectrons were collected at a 55° photoemission angle. Electron kinetic energy was determined by a hemispherical analyzer using a pass energy of 150 V for survey scans ranging from 0 to 1100 eV. To evaluate the chemical composition across the thickness of the plasma-treated superhydrophobic fabric, the iXPS method was performed in an ESCA 2SR XPS instrument (Scienta Omicron), using a nonmonochromatic Al Kα x-rays, generated at a power of 300 W (20 mA; 15 kV). C1s and F1s high-sensitivity spectra were collected at 200-eV pass energy and 0° photoemission angle from a small analysis spot (200 μm). The analysis spot was moved across the cross section of the fabric (from the back spot area to the top spot area) at steps of 51.4 μm. A flood gun was used for charge neutralization of all the samples. Data analysis was performed on CasaXPS software.

Thermal analysis

A thermogravimetric analyzer (TGA 500, TA Instruments) was used to determine the amount of TiO_2 nanoparticles deposited on the treated fabric. Each sample (5 to 10 mg) was placed in an alumina ceramic crucible and thermally heated from 30° to 990°C in a nitrogen gas medium with a heating rate of 10°C/min. The weight percentage of TiO_2 nanoparticles was estimated by calculating the difference between the remaining weight of pristine cotton fabric and TiO_2/PFOTES-coated fabric.

Water dripping test

Water droplets of ~20 μl per droplet were dripped onto either top or back sides of the horizontally laid superhydrophobic finished fabrics after selective plasma treatment. Continuous water droplet supplied from a syringe pump (SK-500 III, Shenzhen Shenke Medical, China) with a flow rate of 10 μl/min was dripped by a needle on either top or back sides of the 45° inclined laid fabrics.

Water flux test

A homemade device was set up to measure the breakthrough pressure of the fabrics (fig. S7A) (*12*). The device includes a water source from a syringe pump, a hollow syringe cylinder with the bottom end attached with the testing fabric, and an underneath glass bottle collector. During the test, the fluid rate was set to 0.05, 0.09, 0.4, and 0.95 ml/min, respectively. The breakthrough pressure was recorded as the minimum pressure under which the water starts to pass through the fabric.

Water shower test

The water transport properties were further measured by a water shower test. A testing fabric was capped over on a 20-ml glass vessel loaded with ~1 g of blue silica gel beads. The vessel was then showered by an eye shower for 10 s, and the color of inside silica gel beads was checked to find whether there was water transported through the fabric. Both top and back sides of the fabrics were tested to check the transport difference.

Artificial sweat test

Continuous artificial sweat droplet supplied from a syringe pump (SK-500 III, Shenzhen Shenke Medical, China) with a flow rate of 10 μl/min was also dripped by a needle on either top or back sides of the fabric. The fabric was originally laid horizontally to test the droplet behavior against the gravity and then was rotated into different angles to check the transport and roll-off behaviors. The artificial sweat was prepared according to ISO 3160-2, which comprises NaCl (20 g/liter), NH_4Cl (17.5 g/liter), acetic acid (5 g/liter), and D,L-lactic acid (15 g/liter), with the pH adjusted to 4.7 by NaOH (*37*, *38*).

Mechanical test

Tensile tests of the cotton fabric before and after superhydrophobic finishing and plasma treatment were carried out on a uniaxial load test machine (model no. 5566, Instron, USA) according to American Society for Testing and Materials (ASTM) D5034-09 standards, and fracture stress (σ_f), fracture strain (ε_f), and Young's modulus (E) were determined. Four specimens (25 mm × 10 mm) were measured for each fabric sample. The thickness of each sample was measured using a vernier caliper at five different locations. The average thickness of pristine cotton fabric, superhydrophobic finished fabric, and superhydrophobic finished fabric after selective plasma treatment was found to be 0.30, 0.32, and 0.32 mm, respectively. The gauge length was set to 20 mm, and the cross-head speed was 300 mm/min. Each test was stopped until the load was recovered to 90% of the peak load.

WVTR measurement

The WVTR of the cotton fabric before and after superhydrophobic finishing and plasma treatment was measured with an upright cup method according to BS 7209 (*39*, *40*), with a modified size sample and temperature at 35°C. Each sample was cut into a circular sharp with a diameter around 25 mm and attached firmly on top of a 20-ml glass vessel (diameter 16 mm) via an adhesive. Each cup contained ~20 g of deionized water inside. The vessels were then placed on a heater at a temperature of 35°C and tested over 1 hour to determine the water mass loss over the time as the WVTR. The WVTR (g/m^2 per hour) was calculated by $WVTR = M/(At)$, where M is the loss in mass (g), t is the time duration (hours), and A is the area of the exposed test fabric that is equal to the area of the vessel caliber (m^2).

Air permeability measurement

Air permeability of various fabrics was tested via a gas permeability module on Capillary Flow Porometer 7.0 (CFP-1100-AEHXL, Porous Materials Inc., USA) (*41*). Samples were cut into circular sharps with a diameter of ~25 mm, placed gently in the chamber, and fixed by

the seal O-ring (an inner diameter of 18.3 mm and an outer diameter of 25 mm) and the adapter plates. During the test, the air pressure will increase, and the flow through and pressure drop across the sample will be measured. From the affiliated software, an average Darcy's permeability constant (Darcy or cm^2; 1 Darcy = 9.87×10^{-9} cm^2) will be obtained for each sample according to sample thickness, diameter, air flow, and pressure.

Abrasion test

Abrasion resistance was evaluated according to ASTM D 4966 using the SDL Atlas Martindale Abrasion Tester. Specimens were cut into a circle with 1.5 inches in diameter and loaded into the tester holders using a polyurethane backing. A fixed weight was loaded to give a pressure of 1.31 ± 0.03 psi (9 ± 0.2 kPa) on each specimen. The machine was then set to run for up to 25,000 cycles at 47.5 rpm. Fabrics after abrasion test were evaluated on wettability, nanoparticle content, and surface morphologies by CA test, TGA, and SEM, respectively.

Data analysis

The experimental data were analyzed using analysis of variance (ANOVA). The significance level was set at $P < 0.05$. Results were reported as means ± SD.

SUPPLEMENTARY MATERIALS

Supplementary material for this article is available at http://advances.sciencemag.org/cgi/content/full/6/14/eaaz0013/DC1

REFERENCES AND NOTES

1. M. Manshahia, A. Das, High active sportswear—A critical review. *Indian J. Fibre Text. Res.* **39**, 441–449 (2014).
2. R. Paul, *High Performance Technical Textiles* (John Wiley & Sons, ed. 1, 2019).
3. D. J. Gohlke, J. C. Tanner, Gore-Tex waterproof breathable laminates. *J. Coated Fabrics* **6**, 28–38 (1976).
4. A. Mukhopadhyay, V. K. Midha, A review on designing the waterproof breathable fabrics part II: Construction and suitability of breathable fabrics for different uses. *J. Ind. Text.* **38**, 17–41 (2008).
5. J. Fan, Y. S. Chen, Measurement of clothing thermal insulation and moisture vapour resistance using a novel perspiring fabric thermal manikin. *Meas. Sci. Technol.* **13**, 1115–1123 (2002).
6. A. R. Parker, C. R. Lawrence, Water capture by a desert beetle. *Nature* **414**, 33–34 (2001).
7. L. Zhai, M. C. Berg, F. Ç. Cebeci, Y. Kim, J. M. Milwid, M. F. Rubner, R. E. Cohen, Patterned superhydrophobic surfaces: Toward a synthetic mimic of the Namib Desert beetle. *Nano Lett.* **6**, 1213–1217 (2006).
8. Y. Zheng, H. Bai, Z. Huang, X. Tian, F.-Q. Nie, Y. Zhao, J. Zhai, L. Jiang, Directional water collection on wetted spider silk. *Nature* **463**, 640–643 (2010).
9. J. Ju, H. Bai, Y. Zheng, T. Zhao, R. Fang, L. Jiang, A multi-structural and multi-functional integrated fog collection system in cactus. *Nat. Commun.* **3**, 1247 (2012).
10. Y. Zhao, H. Wang, H. Zhou, T. Lin, Directional fluid transport in thin porous materials and its functional applications. *Small* **13**, (2017).
11. J. Li, Y. Song, H. Zheng, S. Feng, W. Xu, Z. Wang, Designing biomimetic liquid diodes. *Soft Matter* **15**, 1902–1915 (2019).
12. D. Shou, J. Fan, An all hydrophilic fluid diode for unidirectional flow in porous systems. *Adv. Funct. Mater.* **28**, 1800269 (2018).
13. E. A. Arens, H. Zhang, The skin's role in human thermoregulation and comfort, in *Thermal and Moisture Transport in Fibrous Materials*, N. Pan, P. Gibson, Eds. (Woodhead Publishing Limited, 2006), pp. 560–602.
14. E. Proksch, J. M. Brandner, J. M. Jensen, The skin: An indispensable barrier. *Exp. Dermatol.* **17**, 1063–1072 (2008).
15. Y. Lu, S. Sathasivam, J. Song, C. R. Crick, C. J. Carmalt, I. P. Parkin, Robust self-cleaning surfaces that function when exposed to either air or oil. *Science* **347**, 1132–1135 (2015).
16. D. Miao, Z. Huang, X. Wang, J. Yu, B. Ding, Continuous, spontaneous, and directional water transport in the trilayered fibrous membranes for functional moisture wicking textiles. *Small* **14**, 1801527 (2018).
17. X. Wang, Z. Huang, D. Miao, J. Zhao, J. Yu, B. Ding, Biomimetic fibrous murray membranes with ultrafast water transport and evaporation for smart moisture-wicking fabrics. *ACS Nano* **13**, 1060–1070 (2019).
18. H. Zhou, H. Wang, H. Niu, T. Lin, Superphobicity/philicity Janus fabrics with switchable, spontaneous, directional transport ability to water and oil fluids. *Sci. Rep.* **3**, 2964 (2013).
19. M. Ge, C. Cao, J. Huang, X. Zhang, Y. Tang, X. Zhou, K. Zhang, Z. Chen, Y. Lai, Rational design of materials interface at nanoscale towards intelligent oil–water separation. *Nanoscale Horiz.* **3**, 235–260 (2018).
20. D. Liang, Z. Lu, H. Yang, J. T. Gao, R. Chen, Novel asymmetric wettable AgNPs/chitosan wound dressing: In vitro and in vivo evaluation. *ACS Appl. Mater. Interfaces* **8**, 3958–3968 (2016).
21. L. Shi, X. Liu, W. Wang, L. Jiang, S. Wang, A self-pumping dressing for draining excessive biofluid around wounds. *Adv. Mater.* **31**, 1804187 (2019).
22. S. M. Montgomery, K. L. Adams, L. Rebenfeld, Directional inplane permeabilities of geotextiles. *Geotext. Geomembr.* **7**, 275–292 (1988).
23. A. Miszkowska, S. Lenart, E. Koda, Changes of permeability of nonwoven geotextiles due to clogging and cyclic water flow in laboratory conditions. *Water* **9**, 660 (2017).
24. J. Feng, J. P. Rothstein, One-way wicking in open micro-channels controlled by channel topography. *J. Colloid Interface Sci.* **404**, 169–178 (2013).
25. E. Fu, S. A. Ramsey, P. Kauffman, B. Lutz, P. Yager, Transport in two-dimensional paper networks. *Microfluid. Nanofluidics* **10**, 29–35 (2011).
26. B. Xiao, J. Fan, F. Ding, A fractal analytical model for the permeabilities of fibrous gas diffusion layer in proton exchange membrane fuel cells. *Electrochim. Acta* **134**, 222–231 (2014).
27. A. Tourovskaia, T. Barber, B. T. Wickes, D. Hirdes, B. Grin, D. G. Castner, K. E. Healy, A. Folch, Micropatterns of chemisorbed cell adhesion-repellent films using oxygen plasma etching and elastomeric masks. *Langmuir* **19**, 4754–4764 (2003).
28. H. Wang, J. Ding, L. Dai, X. Wang, T. Lin, Directional water-transfer through fabrics induced by asymmetric wettability. *J. Mater. Chem.* **20**, 7938–7940 (2010).
29. C. X. Wang, Y. Ren, Y. P. Qiu, Penetration depth of atmospheric pressure plasma surface modification into multiple layers of polyester fabrics. *Surf. Coat. Technol.* **202**, 77–83 (2007).
30. J. Wu, Z. Mao, L. Han, J. Xi, Y. Zhao, C. Gao, Directional migration of vascular smooth muscle cells guided by synergetic surface gradient and chemical pattern of poly(ethylene glycol) brushes. *J. Bioact. Compat. Polym.* **28**, 605–620 (2013).
31. C. X. Wang, Y. Liu, H. L. Xu, Y. Ren, Y. P. Qiu, Influence of atmospheric pressure plasma treatment time on penetration depth of surface modification into fabric. *Appl. Surf. Sci.* **254**, 2499–2505 (2008).
32. H. Ohshima, H. Matsubara, Surface tension of electrolyte solutions. *Colloid Polym. Sci.* **282**, 1044–1048 (2004).
33. W. L. Hsin, Y.-J. Sheng, S.-Y. Lin, H.-K. Tsao, Surface tension increment due to solute addition. *Phys. Rev. E* **69**, 031605 (2004).
34. L. Lao, L. Fu, G. Qi, E. P. Giannelis, J. Fan, Superhydrophilic wrinkle-free cotton fabrics via plasma and nanofluid treatment. *ACS Appl. Mater. Interfaces* **9**, 38109–38116 (2017).
35. M. Y. Cao, K. Li, Z. Dong, C. Yu, S. Yang, C. Song, K. Liu, L. Jiang, Superhydrophobic "Pump": Continuous and spontaneous antigravity water delivery. *Adv. Funct. Mater.* **25**, 4114–4119 (2015).
36. K. P. Tang, J. T. Fan, J. F. Zhang, M. K. Sarkar, C. W. Kan, Effect of softeners and crosslinking conditions on the performance of easy-care cotton fabrics with different weave constructions. *Fiber Polym.* **14**, 822–831 (2013).
37. F. Benito-Lopez, S. Coyle, R. Byrne, V. F. Curto, D. Diamond, "Sweat-on-a-Chip": Analysing sweat in real time with disposable micro-devices, in *2010 IEEE SENSORS* (IEEE, 2010), pp. 160–163.
38. G. Xiao, J. He, X. Chen, Y. Qiao, F. Wang, Q. Xia, L. Yu, Z. Lu, A wearable, cotton thread/paper-based microfluidic device coupled with smartphone for sweat glucose sensing. *Cellulose* **26**, 4553–4562 (2019).
39. J. Huang, X. Qian, Comparison of test methods for measuring water vapor permeability of fabrics. *Text. Res. J.* **78**, 342–352 (2008).
40. M. Kim, Y. S. Wu, E. C. Kan, J. Fan, Breathable and flexible piezoelectric ZnO@PVDF fibrous nanogenerator for wearable applications. *Polymers* **10**, 745 (2018).
41. J. A. Fernando, D. D. L. Chung, Pore structure and permeability of an alumina fiber filter membrane for hot gas filtration. *J. Porous Mater.* **9**, 211–219 (2002).

Acknowledgments: This work made use of the Cornell Center for Materials Research Facilities supported by NSF MRSEC program (DMR-1719875). This work also made use of Cornell Energy Systems Institute (CESI). We also acknowledge M. Frey for providing the usage of plasma etcher, H. Bai for providing help of scheme design, and M. Salim for imaging XPS assistance. **Funding:** This work was supported by J.T.F.'s faculty fund at Cornell, PolyU (1-ZE1H), RGC (PolyU 252029/19E), and ITF (ITS/093/19). **Author contributions:** J.T.F., L.L., and D.S. conceived the idea and designed the research. L.L. and Y.S.W. formulated the fabrication process. L.L. performed the experiments. D.S. conducted the mechanism modeling. L.L. and D.S. analyzed

and interpreted the results. The manuscript was written through the contributions of all authors. All authors have given approval to the final version of the manuscript. **Competing interests:** L.L., D.S., and J.T.F. are inventors on a pending patent related to this work filed by Cornell University (application no. 16/663,135). The authors declare no other competing interests. **Data and materials availability:** All data needed to evaluate the conclusions in the paper are present in the paper and/or the Supplementary Materials. Additional data related to this paper may be requested from the authors.

Submitted 5 August 2019
Accepted 9 January 2020
Published 3 April 2020
10.1126/sciadv.aaz0013

Citation: L. Lao, D. Shou, Y. S. Wu, J. T. Fan, "Skin-like" fabric for personal moisture management. *Sci. Adv.* **6**, eaaz0013 (2020).